Atmos. Chem. Phys., 6, 1075–1089, 2006
www.atmos-chem-phys.net/6/1075/2006/

Atmospheric Chemistry and Physics

Estimating the NO_x produced by lightning from GOME and NLDN data: a case study in the Gulf of Mexico

S. Beirle[1], N. Spichtinger[2], A. Stohl[3], K. L. Cummins[4], T. Turner[4], D. Boccippio[5], O. R. Cooper[6], M. Wenig[7], M. Grzegorski[1], U. Platt[1], and T. Wagner[1]

[1]Institut für Umweltphysik, Universität Heidelberg, Germany
[2]Department of Ecology, Technical University of Munich, Germany
[3]Norsk institutt for luftforskning NILU, Kjeller, Norway
[4]Vaisala, Tucson, Arizona, USA
[5]Global Hydrology and Climate Center, NASA Marshall Space Flight Center, Huntsville, Alabama, USA
[6]NOAA Aeronomy Laboratory, Boulder, Colorado, USA
[7]NASA Goddard Space Flight Center, Greenbelt, Maryland, USA

Received: 12 October 2005 – Published in Atmos. Chem. Phys. Discuss.: 9 November 2005
Revised: 1 March 2006 – Accepted: 20 March 2006 – Published: 3 April 2006

Abstract. Nitrogen oxides (NO_x=NO+NO_2) play an important role in tropospheric chemistry, in particular in catalytic ozone production. Lightning provides a natural source of nitrogen oxides, dominating the production in the tropical upper troposphere, with strong impact on tropospheric ozone and the atmosphere's oxidizing capacity. Recent estimates of lightning produced NO_x (LNO_x) are of the order of 5 Tg [N] per year with still high uncertainties in the range of one order of magnitude.

The Global Ozone Monitoring Experiment (GOME) on board the ESA-satellite ERS-2 allows the retrieval of tropospheric column densities of NO_2 on a global scale. Here we present the GOME NO_2 measurement directly over a large convective system over the Gulf of Mexico. Simultaneously, cloud-to-ground (CG) flashes are counted by the U.S. National Lightning Detection Network (NLDN™), and extrapolated to include intra-cloud (IC)+CG flashes based on a climatological IC:CG ratio derived from NASA's space-based lightning sensors. A series of 14 GOME pixels shows largely enhanced column densities over thick and high clouds, coinciding with strong lightning activity. The enhancements can not be explained by transport of anthropogenic NO_x and must be due to fresh production of LNO_x. A quantitative analysis, accounting in particular for the visibility of LNO_x from satellite, yields a LNO_x production of 90 (32–240) moles of NO_x, or 1.3 (0.4–3.4) kg [N], per flash. If simply extrapolated, this corresponds to a global LNO_x production of 1.7 (0.6–4.7) Tg [N]/yr.

1 Introduction

Nitrogen oxides (NO_x=NO+NO_2) play an important role in atmospheric chemistry. In the troposphere, they drive catalytic ozone production. Furthermore, NO_x controls OH concentration and thus the atmosphere's oxidizing capacity. In total, about 44 Tg [N] of nitrogen oxides are released annually, half of which are due to fossil fuel combustion (Lee et al., 1997). Further large sources are biomass burning (≈8 Tg [N]/yr) and soil emissions (≈7 Tg [N]/yr).

Lightning produced NO_x (hereafter denoted by LNO_x) is estimated to contribute about 5 Tg [N]/yr (Lee et al., 1997). However, the best estimates of recently published studies still vary between 0.9 and 12.2 Tg [N]/yr (e.g. Nesbitt et al., 2000; Price et al., 1997), and the given uncertainties typically are one order of magnitude. Thus lightning is the least known important source of nitrogen oxides. Furthermore, in contrast to other sources, LNO_x is directly released also in the upper troposphere where background levels of NO_x are low and the lifetime of NO_x is of the order of a few days, i.e. several times longer than for the boundary layer (≈hours). Hence both tropospheric ozone as well as OH concentrations are particularly sensitive to LNO_x (e.g. Stockwell et al., 1999; Labrador et al., 2004). For the correct assessment of NO_x inventories, a prerequisite for reliable model calculations of atmospheric chemistry, better knowledge on LNO_x is essential.

Over the last decades, several studies using different methods have been performed to estimate LNO_x production. A common bottom-up approach is to assess (a) the production of NO_x per energy unit, (b) the released energy per flash and

Correspondence to: S. Beirle
(beirle@iup.uni-heidelberg.de)

Published by Copernicus GmbH on behalf of the European Geosciences Union.

(c) the global frequency of flashes, and to estimate the global LNO_x production as the product of these quantities. Literature values range over some orders of magnitude, as a result of the many assumptions and necessary extrapolations of laboratory measurements involved (see Price et al., 1997 for an overview). Further complications arise from differences in cloud-to-ground (CG) and intra-cloud (IC) flashes. IC flashes are more frequent, but CG flashes are more energetic and hence produce more LNO_x per flash, concrete numbers still being under discussion (see e.g. Fehr et al., 2004 and references therein).

In-situ measurements of LNO_x have been performed in several aircraft campaigns, where global LNO_x estimates range from 0.9–220 Tg [N] per year (for an overview see Huntrieser et al., 1998). In their own study, Huntrieser et al. (1998) found annual LNO_x production to be 4 (0.3–22) Tg [N]. More recently, Huntrieser et al. (2002) analyzed European thunderstorms recorded during the EULINOX project in detail and estimated the annual LNO_x production at 3 Tg [N].

Also chemical transport models (CTMs) have been used to restrict the range of LNO_x production by comparing modeled NO_x concentrations for different LNO_x scenarios with local field measurements. The studies by Levy et al. (1996), Tie et al. (2002), and Jourdain and Hauglustaine (2001) find about 5 Tg [N], 2–6 Tg [N], and 3.5–7 Tg [N], respectively, as best estimates for yearly global LNO_x production.

The fact that several independent approaches result in a global LNO_x production of about 5 Tg [N] per year confirms that at least the order of magnitude can be expected to be correct. However, the uncertainties of the different methods are still quite high, indicating the need for further, independent information.

Satellite based measurements of atmospheric trace gases are a powerful addition to measurements from conventional platforms. They provide a global dataset with uniform instrumental features, and meanwhile span several years of measurements. The spectral data from the Global Ozone Monitoring Instrument GOME allow to determine column densities of various trace gases, in particular NO_2 (e.g. Leue et al., 2001; Richter and Burrows, 2002; Martin et al., 2002). By estimating and subtracting the stratospheric column, and accounting for radiative transfer, tropospheric NO_2 column densities can be derived from GOME data (e.g. Leue et al., 2001; Richter and Burrows, 2002; Beirle et al., 2003; Martin et al., 2003; Boersma et al., 2004).

The global view offered by satellite observations provides new insights on the spatial distribution of NO_x sources (e.g. Velders et al., 2001; Leue et al., 2001; Richter and Burrows, 2002; Martin et al., 2003; Beirle et al., 2004b, d). The analysis of characteristic temporal and spatial patterns has been used to identify and quantify the magnitude of different NO_x sources, e.g. continental anthropogenic emissions (Martin et al., 2003; Beirle et al., 2003), ship emissions (Beirle et al., 2004c; Richter et al., 2004), biomass burning (e.g. Richter and Burrows, 2002; Spichtinger et al., 2004), or soil emissions (Jaeglé et al., 2004).

On account of this successful use of GOME NO_2 data it is obvious to investigate LNO_x from GOME as well. However, while the signal of e.g. industrial sources is often unambiguous, the clear detection of LNO_x is more complex: In contrast to anthropogenic emissions, the occurrence of lightning is highly variable in space and time. Furthermore, lightning occurs predominantly in the late afternoon or evening, whereas GOME measurements take place before local noon. Due to the longer lifetime of NO_x of several days in the upper troposphere (Jaegle et al., 1998), LNO_x can accumulate to detectable amounts, but these aged LNO_x plumes are diluted, and the spatial patterns are faint compared to the sharp NO_2 maxima of boundary layer sources.

Moreover, thunderstorms are extreme weather events. As a consequence of deep convection and downdraft motions, the profile of lightning produced NO_x as well as NO_x from boundary layer sources is strongly modified. A large fraction of the produced LNO_x is uplifted in the anvil, resulting in a pronounced C-shaped profile of LNO_x (e.g. Pickering et al., 1998; Fehr et al., 2004). Furthermore thunderstorms are accompanied by high and thick clouds. Both factors strongly affect the visibility of NO_2 from satellite.

Despite these difficulties, some studies report a correlation of lightning activity and increased NO_2 column densities. Zhang et al. (2000) used NO_2 data from the Upper Atmosphere Research Satellite (UARS) to substantiate a (rather qualitative) link between lightning activity and high levels of NO_2 in the upper troposphere. Richter and Burrows (2002) report enhanced NO_2 column densities above clouds due to lightning for Africa. Beirle et al. (2004a) analyzed correlations of monthly means of lightning activity and GOME NO_2 column densities for Australia and estimated the global LNO_x production as 2.7 (0.8–14) Tg [N]/yr. Boersma et al. (2005) compared the 1997 GOME NO_2 column densities to model output for different tropical regions and give a range for annual LNO_x production of 1.1–6.4 Tg [N]/yr.

Besides these statistical approaches, studies on particular lightning events using GOME data have also been reported. Hild et al. (2000) analyzed a lightning event south from Africa coinciding with enhanced NO_2 column densities from GOME measurements nearby. Choi et al. (2005) found evidence for lightning enhancements of NO_2 over North America and the western North Atlantic.

Here we present the direct GOME measurement of enhanced NO_2 column densities over a large convective system in the Gulf of Mexico, while flashes are counted by the U.S. National Lightning Detection Network simultaneously.

2 Methods

2.1 NO_2 column densities from GOME

For this study we have used data from the Global Ozone Monitoring Experiment (GOME) (Burrows et al., 1999). GOME orbits the earth onboard the ERS-2 satellite, flying in a sun-synchronous nearly polar orbit and crossing the equator at 10:30 a.m. local time. The GOME instrument consists of four spectrometers measuring the radiation reflected by the earth in the UV/vis spectral range (240–790 nm) with a resolution of 0.2–0.4 nm. The extent of a GOME ground pixel is 320 km east-west and 40 km north-south (size and orientation of a GOME pixel are illustrated in Fig. 1). Within three days, global coverage is achieved at the equator.

Applying the established Differential Optical Absorption Spectroscopy (DOAS) (Platt, 1994), the GOME spectra are analyzed at 430–450 nm to derive slant column densities, i.e. integrated concentrations along the light path, of NO_2 (Wagner, 1999). The stratospheric fraction of the total NO_2 column at a given latitude is estimated over the remote Pacific at same latitude (e.g. Richter and Burrows, 2002) where the tropospheric pollution is negligible. Assuming the stratospheric NO_2 being independent on longitude, the stratospheric column can be subtracted from the total column, resulting in tropospheric (excess) slant column densities (abbreviated as TSCDs and denoted with S hereafter) of NO_2.

The slant column densities are commonly converted to vertical column densities (VCDs), i.e. vertically integrated concentrations, via the air mass factor (AMF) (Solomon et al., 1987). The AMF (A) is defined as the ratio of SCD (S) and VCD (V), hence VCDs are derived according to

$$V = S/A. \tag{1}$$

The stratospheric AMF depends mainly on the geometric light path, i.e. the solar zenith angle. In the troposphere, the effects of Rayleigh and Mie scattering become more important. Hence tropospheric AMFs depend on the trace gas profile, the ground albedo, the aerosol load and especially on clouds. Tropospheric AMFs are derived from radiative transfer modeling. According to Richter and Burrows (2002), Fig. 2, the tropospheric AMF at 437.5 nm is close to 1 for cloud free conditions, a homogeneous mixing in a boundary layer of 1.5 km height, maritime aerosols, and a surface albedo of 0.05. We apply the tropospheric AMF from Richter and Burrows (2002) for the cloud free pixels of our study.

Conditions for NO_2 from lightning, however, are quite different: deep convection causes high and thick clouds and leads to modified vertical NO_x profiles. Both factors strongly affect the NO_2 visibility from satellite. The calculation of appropriate AMFs for NO_2 from lightning in the current study is described in Sect. 4.2 in detail.

After subtraction of the stratospheric column and AMF correction, the final data products are tropospheric VCDs that are abbreviated as TVCDs and denoted with V hereafter.

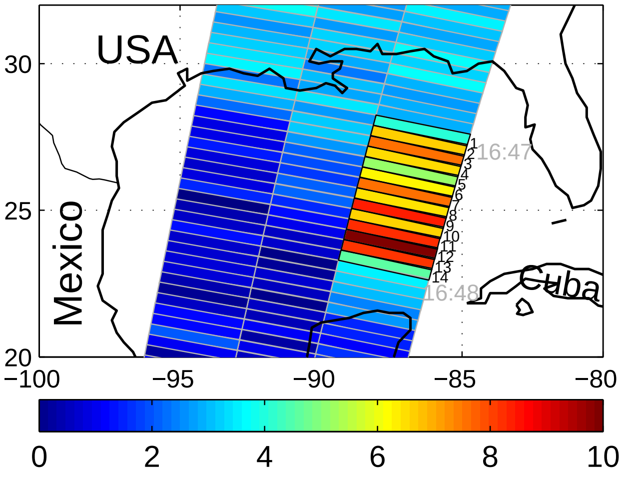

Fig. 1. GOME NO_2 TSCDs (10^{15} molec/cm^2) on 30 August 2000 in the Gulf of Mexico. From 16:47–16:48, a series of 14 eastern pixels (marked in black and numbered) shows enhanced values above 4×10^{15} molec/cm^2

2.2 Cloud data

Cloud information is essential for the calculation of AMFs for given satellite measurements as they shield the boundary layer, but enhance the visibility for absorbers at the cloud top due to multiple scattering and above due to the high albedo. Cloud data are retrieved on global scale from various satellite borne VIS, IR and microwave sensors. Hourly infrared satellite images were available from the NOAA GOES-8 geostationary satellite. Channel 4 of the imager on board the satellite measures the intensity of the radiation emitted by the Earth between 10.2 and 11.2 μm, providing the temperature of the Earth's surface and cloud tops at 4 km resolution.

In addition to data from such meteorological satellites, cloud information can be obtained from the GOME measurement itself. This has the advantage that the cloud data match the NO_2 observation exactly in space and time. At the IUP Heidelberg, cloud fractions are derived from intensity measurements of the polarization monitoring devices (PMDs) by the HICRU algorithm (Grzegorski et al., 2006). The spatial PMD resolution (20×40 km^2) is 16 times higher than that of the GOME groundpixel. Thus HICRU provides also information on cloud heterogeneity across the GOME pixel.

2.3 Lightning detection: NLDN

The U.S. National Lightning Detection Network (NLDN™) was the source of the archived CG lightning information. At the time of the case evaluated in this study (August 2000), the NLDN was comprised of 106 ground-based electromagnetic sensors operating in the VLF/LF frequency range. These sensors were configured to detect emissions produced by return strokes in CG lightning, and to locate these discharges using

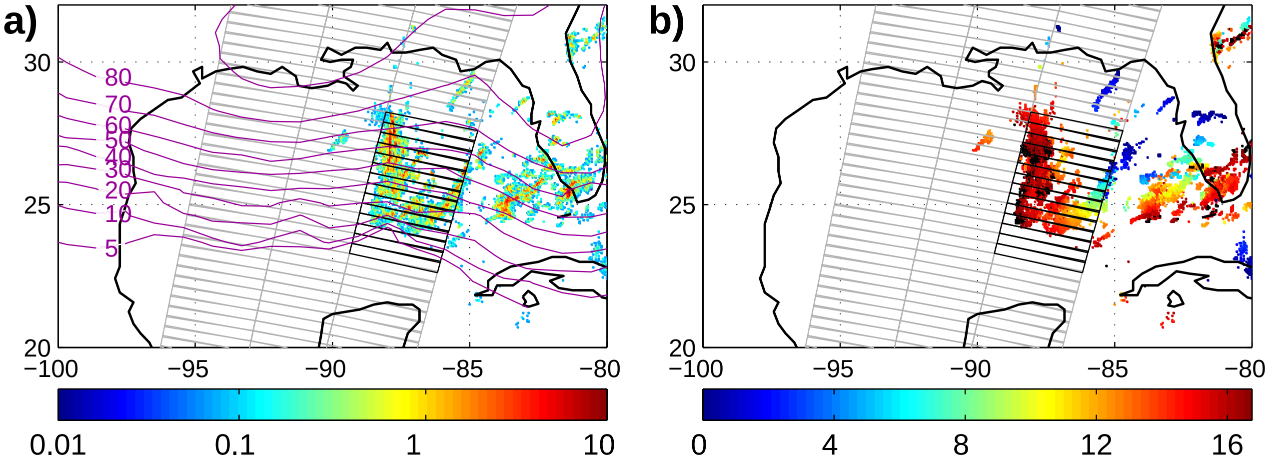

Fig. 2. Lightning observations on 30 August 2000 from NLDN. **(a)** Number of detected flashes per km^2 before the GOME measurement. Purple contour lines display the NLDN detection efficiency. The GOME pixel grid is added as a reference for both subplots. **(b)** Time (UTC) of the last flash detected by the NLDN previous to ERS-2 overpass (16:48). Black dots mark lightning from 16:40–16:48.

a combination of time-of-arrival and magnetic direction finding techniques (Cummins et al., 1998). The median location accuracy was 500 m, and the flash detection efficiency for events with peak current above 5 kA was estimated to be 80–90% over the continental U.S., falling off steadily out to about 500 km outside the network perimeter. Due to the falloff of detection efficiency in the area of interest for this study, model-based corrections provided by Vaisala Thunderstorm (Tucson, Arizona, see http://www.vaisala.com/) were employed to correct for performance fall-off.

2.4 Transport modeling: FLEXPART

GOME measurements at a given location are “snapshots” taken once every 3 days. For the clear identification of NO_x sources, effects of transport have to be taken into account. In this study, transport simulations of various NO_x tracers (i.e. anthropogenic NO_x, aged and fresh LNO_x, see Sect. 4.3) are performed with the Lagrangian particle dispersion model FLEXPART (version 6.2) (Stohl et al., 1998, 2005) (see also http://zardoz.nilu.no/~andreas/flextra+flexpart.html). FLEXPART simulates the transport and dispersion of non-reactive tracers by calculating the trajectories of a multitude of particles. It was validated with data of various large scale tracer experiments (Stohl et al., 1998) and the model results were compared to different kinds of satellite data. In detail, with respect to this paper, FLEXPART was already successfully used to study the advection of forest fire NO_x from Canada to Europe (Spichtinger et al., 2001), to simulate a power plant plume of NO_x traveling from South Africa towards Australia (Wenig et al., 2003), and to model the transport of anthropogenic NO_x from the US eastcoast towards Europe within a meteorological bomb (Stohl et al., 2003).

FLEXPART is driven by data from the European Centre for Medium-Range Weather Forecasts (ECMWF, 1995). The data set has a temporal resolution of 3 hours (analyses at 00:00, 06:00, 12:00, and 18:00 UTC; 3-h forecasts at 03:00, 09:00, 15:00, and 21:00 UTC), a horizontal resolution of $1^\circ \times 1^\circ$ and 60 vertical levels. Although the ECMWF model reproduces the large-scale effects of convection, they do not resolve individual deep convective cells. In order to account for subgrid-scale convection, FLEXPART was recently equipped with a convective parameterization scheme (Emanuel and Zivkovic-Rothman, 1999; Emanuel, 1991).

FLEXPART does not model chemical processes. The chemical decay of NO_x is considered by assigning the NO_x tracer with a constant e-folding lifetime. More information on the NO_x tracers simulated (anthropogenic NO_x, aged and fresh LNO_x and the respective e-folding lifetime) is given in Sect. 4.3.

3 Case study: a thunderstorm in the Gulf of Mexico

Lightning frequency is highest in late afternoon, while GOME measurements are taken around 10:30 a.m. local time. Nevertheless, the direct observation of lightning during an ERS-2 overpass occasionally occurs within the large amount of GOME data. An unique event of GOME capturing LNO_x just produced is found on 30 August 2000 over the Gulf of Mexico: a sequence of about 14 pixels, measured at 16:47–16:48 UTC, shows high NO_2 TSCDs (Fig. 1) that by far exceed normal levels over ocean.

These high TSCDs coincide with a strong convective system causing high lightning activity. Figure 2a depicts the flashes detected by the NLDN on 30 August 2000 before the ERS-2 overpass at 16:48 UTC. For better comparison, the

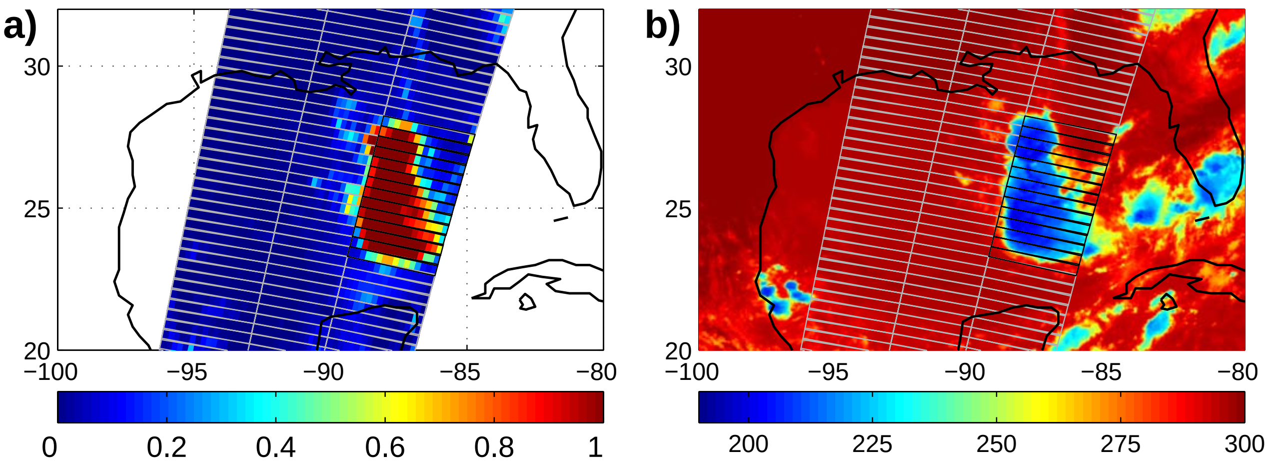

Fig. 3. Cloud observations on 30 August 2000. **(a)** Cloud fraction derived from GOME PMD measurements (HICRU). **(b)** Cloud top temperature (K) from IR measurements (GOES) at 16:15 UTC. The temperatures <220 (210) K correspond to cloud top heights >12.5 (14) km. The GOME pixel grid is added as a reference.

GOME pixel grid is overlaid in all subplots. To illustrate the temporal coincidence of flashes and GOME measurement, Fig. 2b displays the time of the latest flash occurrence. More than half of the detected flashes occurred less than 3 h before ERS-2 overpass. Black dots indicate flashes with less than 8 min time difference to the GOME measurement.

Figure 3 shows cloud fractions (a) and cloud top temperatures (b) measured from HICRU and GOES, respectively. HICRU cloud fractions reveal a large cluster of totally clouded PMD pixels, covering an area of ≈500 km north-south and up to 300 km east-west. CTTs from GOES IR measurements at 16:15 UTC are about 200–220 K. This corresponds to cloud top heights of 12.5–16 km according to ECMWF temperature profiles.

This particular event is unprecedented as the lightning activity coincides perfectly with the GOME measurement both in space (the area affected by lightning fits in the eastern GOME pixels) and in time (most flashes have occurred during the last 3 hours). The lightning event took place over sea and remote from polluted regions. The enhanced NO_2 TSCDs can not be explained with transport of anthropogenic emissions (see Sect. 4.3.1). The observed enhanced NO_2 TSCDs are thus unambiguously due to LNO_x. As far as we know, such a clear and direct detection of LNO_x from satellite has never been reported before.

A closer look on the meteorological situation reveals that the convective complex originates from at least two systems of different history. This is illustrated in Fig. 4 that displays hourly GOES CTTs for 30 August. Figure 4a depicts a convective cell at ≈25° N, 85° W, moving WSW and growing during the next hours, becoming the southern part of the large complex detected at 16:15. In fact, this system has already existed several hours before 08:15 (see the blue/cyan dots in Fig. 2b), and was even active on 29 August at the western coast of Florida.

The northern part of the 16:15 complex, however, is rather young. Tracking it back reveals that it stems from a small, singular cell emerging at about 10:15 and growing rapidly (see white marks in Figs. 4c, d, e), and some smaller systems in the north (gray marks in f, g).

For the quantitative estimation of LNO_x given in Sect. 4, we focus our analysis on the northern part of the convective complex, i.e. north from ≈25° N corresponding to the GOME pixels 1–9, since the northern convection cells are young and, thus, in contrast to the southern part, free from aged LNO_x. Furthermore, the detection efficiency (DE) by NLDN is above ≈30% in the northern part, while it decreases to zero further south (see DE contour lines in Fig. 2a). Nevertheless, we add a discussion of the southern part also in Sect. 4.5.

4 Estimate of LNO_x production

We use this particular lightning event to estimate the in-situ produced LNO_x. For this task, the totally produced LNO_x in the northern part of the convective complex is estimated and set in relation to the actual number of flashes.

For this quantitative analysis, the following aspects have to be discussed:

First, the actual number of flashes has to be estimated (Sect. 4.1). The flashes detected by NLDN have to be upscaled since detection efficiency fades over sea and NLDN is insensitive for IC flashes.

Second, the sensitivity of GOME for LNO_x, i.e. the conversion of measured NO_2 TSCDs into NO_x TVCDs, will be discussed in Sect. 4.2.

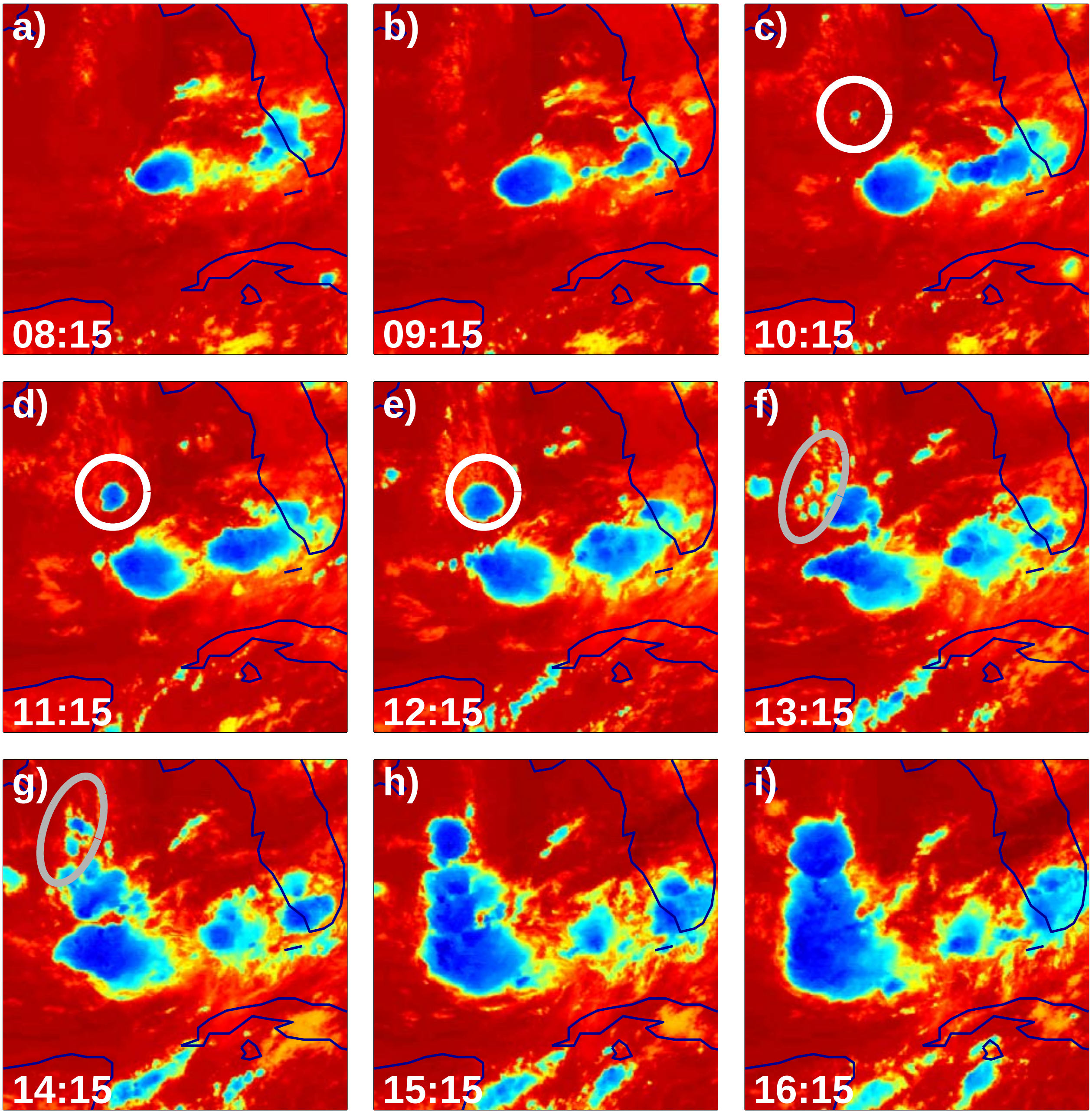

Fig. 4. Evolution of the convective complex as monitored by GOES CTT measurements (all times UTC). Color scale as in Fig. 3b. While the southern part (south from 25° N) has a history of several hours, the northern part just established around 10 a.m. (white marks in **c, d, e**) and after 1 p.m. (gray marks in **f, g**).

Third (Sect. 4.3), the role of transport processes has to be considered. NO_x from anthropogenic sources in the USA, as well as aged LNO_x from the previous days, may be transported into the considered region and interfere with the freshly produced LNO_x. On the other hand, the fresh LNO_x may be partly transported away.

Finally (Sect. 4.4), the total amount of LNO_x produced will be determined and set in relation to the total number of flashes: The resulting LNO_x production (in moles per flash) is

$$E = \frac{\hat{V}^{NO_x} \cdot A}{N_A} \cdot \frac{1}{n} \tag{2}$$

with A being the area of the convective system (Sect. 4.4), N_A being Avogadro's number and n, the total number of flashes (Sect. 4.1).

The corrected NO_x TVCD $\hat{V}$ is calculated as

$$\hat{V}^{NO_x} = (c_{cloud} \cdot S_{GOME}^{NO_2} - S_{anthr}^{NO_2}) \cdot f \cdot c_{aged} \cdot c_{out} \tag{3}$$

The factor c_{cloud} accounts for the fact that the GOME pixels are only partly cloudy, i.e. the true TSCD for the cloudy part of the pixel is slightly higher than the measured TSCD (see Appendix A). The NO_2 TSCD due to anthropogenic emissions $S_{anthr}^{NO_2}$ is estimated in Sect. 4.3.1. The conversion factor f, accounting for the NO_2 AMF and the NO_x partitioning, is derived in Sect. 4.2. The factors c_{aged} and c_{out} account for the impact of aged LNO_x (Sect. 4.3.2) and the loss of fresh LNO_x due to transport (Sect. 4.3.3).

Our results will be compared to literature values and errors will be discussed in detail in Sect. 5.

4.1 How many flashes occurred?

The NLDN detects CG flashes over the US with high detection efficiency (DE). But as the measurement stations are bound to the continent, DE decreases with distance from the shore (see Fig. 2a). In the southern part of the convective complex, the estimated DE is below 5%. The clouded area (Fig. 3) reaches further south than the detected cluster of flashes (Fig. 2a), and it is very likely that flashes at the southern end are not detected at all. For pixels 1–9, however, estimated NLDN DE is above 30%. The number of flashes detected in this area is 4.3×10^4. Scaling this number according to the respective DE results in 9.4×10^4 flashes.

As NLDN did not report IC flashes in 2000, this number refers to CG flashes only. To derive the total number of flashes, the number of IC flashes has to be estimated. Information on the ratio of IC/CG flash frequencies can be derived from long-term comparisons of NLDN measurements with the satellite born instruments OTD (Optical Transient Detector) and LIS (Lightning Imaging Sensor) detecting both IC and CG flashes (Boccippio et al., 2000). According to the climatology for 16 July–14 October, the IC/CG ratio is 2.7 (1.8–4.0) in the considered region. I.e., the number of CG flashes has to be scaled by a factor of 3.7 (2.8–5.0). Hence, we estimate the total number of flashes on 30 August 2000 in the area covered by the GOME pixels 1–9 to be 3.49 (2.64–4.72)$\times 10^5$.

4.2 How to convert NO_2 TSCDs in NO_x TVCDs?

For our study, the starting point are NO_2 TSCDs (S^{NO_2}) derived from GOME spectra. For the quantification of LNO_x, these have to be converted into NO_x TVCDs (V^{NO_x}). The conversion depends on (a) the profile of NO_x, (b) the NO_x partitioning L:=$[NO_2]/[NO_x]$ and (c) the AMF A. Both, A and L are functions of altitude. The overall (effective) AMF A_{eff} is the sum of box AMFs weighted by the NO_2 profile (Eq. B2). The effective partitioning L_{eff} can be calculated as a weighted sum of the height dependent NO_x partitioning (Eq. B8). These equations are derived in Appendix B. The final conversion is

$$V^{NO_x} = f \cdot S^{NO_2} \tag{4}$$

with the conversion factor

$$f = \frac{1}{A_{eff} \cdot L_{eff}} . \tag{5}$$

Information on NO_x profile and partitioning and AMFs is gained from different measurements/model calculations performed for convective cloud conditions.

(a) The profile of NO_x is different for different source types. NO_x from ground sources, here dominated by anthropogenic emissions in the U.S., is mainly located in the boundary layer. Parts of it are lifted due to deep convection, but a large fraction remains in the lowermost kilometers. For anthropogenic NO_x, we apply the vertical profile as derived from FLEXPART simulations (see Sect. 4.3.1).

The situation is different for NO_x from lightning: LNO_x is directly released in the free troposphere, at the very places where updraft takes place. As a result, a large amount of LNO_x is lifted up in the thunderstorm anvil, resulting in profiles often denoted as "C-shaped" (e.g. Pickering et al., 1998; Fehr et al., 2004). Pickering et al. (1998) used a cloud resolving model to construct vertical profiles of LNO_x for use in chemical transport models. We apply the LNO_x profile for tropical marine thunderstorms (Pickering et al., 1998, Table 2). This profile was computed as the mean of three independent case studies. We also apply these three profiles separately (Pickering et al., 1998, Fig. 7) as well as the LNO_x profile published by Fehr et al. (2004) (modified to a cloud top height of 13 km) to investigate the sensitivity of the effective AMF and the correction factor f on the NO_x profile shape.

(b) The partitioning of NO_x in NO and NO_2 depends on several parameters like temperature, O_3 concentration, and actinic flux and thus in particular on height. In the upper troposphere, most NO_x is present as NO due to the low temperatures and high NO_2 photolysis rates. Direct measurements of the NO_x partitioning for cumulonimbus cloud conditions have been performed by Ridley et al. (1994) during 12 measurement flights over New Mexico. Two of these measurements that took place during active thunderstorms are analyzed in detail by Ridley et al. (1996). Conditions for these thunderstorms are similar to the event on 30 August 2000, as they take place in August on similar latitude and close to local noon. We take the NO_2/NO_x ratios given by Ridley et al. (1996, Tables 2 and 4) for the upper core and anvil region and add the missing values below 8 km

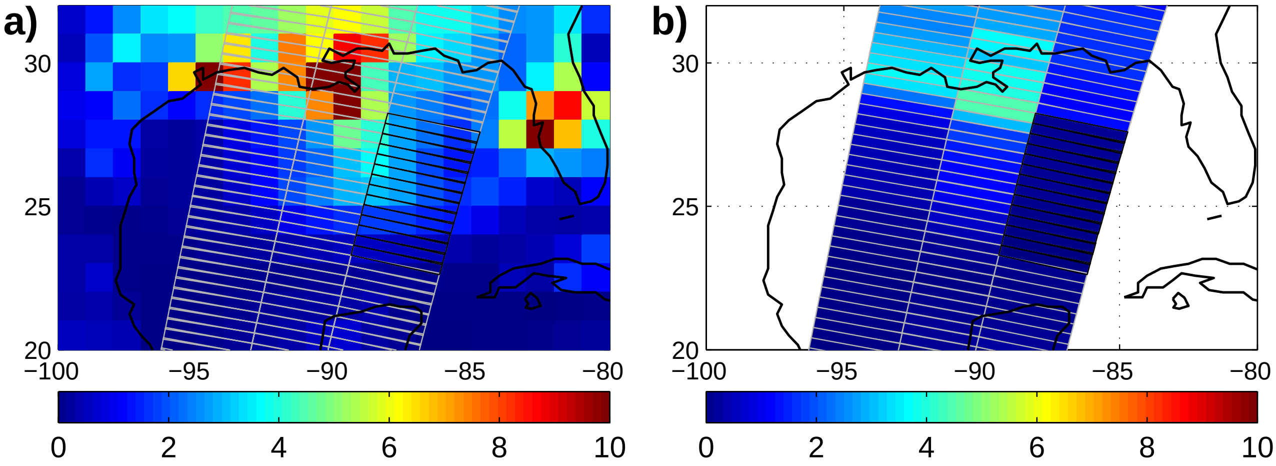

Fig. 5. **(a)** Anthropogenic NO_x TVCD (10^{15} molec/cm^2) as modelled with FLEXPART, assuming a NO_x-lifetime of 24 h and taking emissions from Frost et al. (2005). The GOME pixel grid is indicated as reference. **(b)** FLEXPART NO_x TVCDs converted to NO_2 TSCDs (see Sect. 4.3.1) and regridded on GOME grid for direct comparison with Fig. 1.

from Ridley et al. (1994, Figus. 9 and 11). As we cannot exclude that conditions are different for the convective system under consideration, we allow a rather large range of uncertainty of 50% for the NO_2/NO_x ratio for the anvil region.

(c) As mentioned in Sect. 2.1, the AMF for boundary layer NO_2 under cloud free conditions is about 1 (Richter and Burrows, 2002). But the considered GOME pixels 1-9 are covered by high and thick thunderstorm clouds that strongly impact the visibility of NO_2 from GOME. Clouds have two competing effects: On the one hand, NO_2 below the cloud is shielded. Especially for thick thunderstorm clouds, the boundary layer is effectively invisible from GOME. On the other hand, multiple scattering at the cloud top leads to extended light paths. Thus absorbers at the bright cloud top show an increased visibility from satellite. For the clouded pixels we apply the box AMFs calculated for NO_2 layers of 1 km thickness by Hild et al. (2002, Fig. 3). These box AMFs have been derived for cumulonimbus clouds and thus specifically match conditions for lightning events.

With these settings for the NO_x profile, NO_x partitioning (allowing the calculation of the NO_2 profile) and box AMFs, we get a conversion factor of f=12.49 for anthropogenic NO_x and f=4.02 (2.12–7.14) for LNO_x for the convective system. The resulting effective AMFs are 0.11 and 0.89 (0.52–1.83), the respective effective NO_x partitionings are 0.72 and 0.28 (0.14–0.38).

4.3 What is the impact of transport?

For a quantitative view, the role of transport of NO_x has to be considered. Anthropogenic NO_x, in particular from the US, may have been transported in the considered region and uplifted (Sect. 4.3.1). Also aged LNO_x from lightning events of the previous days may in principle contribute to the detected NO_2 plume, because of the NO_x lifetime of several days in the upper troposphere (Sect. 4.3.2). Finally, the produced LNO_x is partly transported outside the considered area (Sect. 4.3.3).

Transport is modelled with the Lagrangian tracer model FLEXPART (see Sect. 2.4). The capability of FLEXPART to track NO_x transport events has been demonstrated in several studies (Spichtinger et al., 2001; Wenig et al., 2003; Stohl et al., 2003).

4.3.1 Anthropogenic emissions

The transport of NO_x from anthropogenic emissions is simulated with FLEXPART using the inventory for North America compiled by Frost et al. (2006) based on the U.S. EPA NEI-99 (National Emissions Inventory, base year 1999, version 3) (U.S. EPA, 2004a). This inventory was derived at 4-km horizontal resolution from spatial surrogates (U.S. EPA, 2004b) for each U.S. county and Canadian province, and average ozone season day (June through August) county level estimates of on-road, off-road, area, and point sources. The 4-km resolution emissions are also available through a graphics information system interface (Frost and McKeen, 2004). In FLEXPART, emissions were released on the original 4-km grid in regions with high emission densities and from the 300 largest point sources. Grid cells with low emission densities and small point sources were aggregated into lower-resolution grid cells by degrading the resolution in several steps.

The e-folding lifetime for NO_x was set to 24 h, which is a rather conservative assumption, as the lifetime of boundary

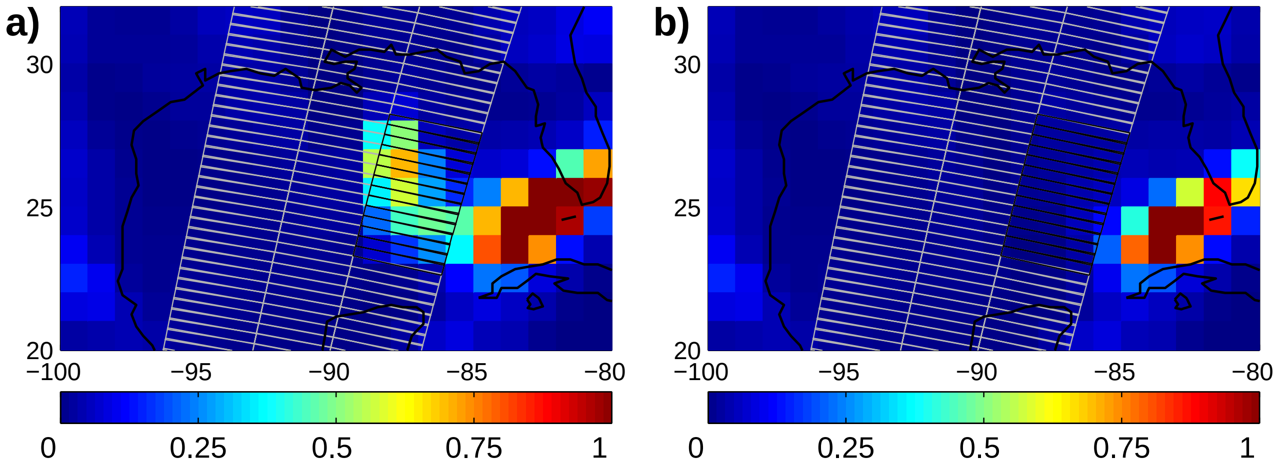

Fig. 6. FLEXPART simulations of LNO_x from 27 August on (artificial units). For every flash detected by NLDN, a fixed amount of NO_x was released. The NO_x lifetime was set to 4 days. Both runs are performed until 30 August 18:00. The GOME pixel grid is added as a reference for both subplots. **(a)** Aged plus fresh LNO_x: simulation accounts for all flashes until 30 August, 16:48. **(b)** Aged LNO_x: simulation accounts for flashes from 27–29 August only. For the considered GOME pixels 1–9, the fraction of aged LNO_x to total LNO_x is 11%.

layer NO_x is of the order of several hours (e.g. Martin et al., 2003; Beirle et al., 2003). The tracer (a total of 5.5 million particles) was permanently released in the box 60°–170° W and 25°-75° N over the time period of 25 to 30 August 2000, i.e. 5 days prior the strong lightning event. To consider the vertical transport within this convective system, FLEXPART was run with the implemented convection scheme.

Figure 5a displays the resulting distribution of anthropogenic NO_x TVCDs in ECMWF resolution of $1° \times 1°$. For direct comparison with GOME measurements (Fig. 1) we regrid the FLEXPART NO_x TVCDs to the GOME grid and calculate TSCDs of anthropogenic NO_2 (Fig. 5b). For this purpose, an effective AMF of 1 (Richter and Burrows, 2002) and an effective NO_2/NO_x ratio of 0.5 were applied for the cloudfree pixels, while for the cloudy pixels the conversion factor f was taken as 12.49, corresponding to A_{eff}=0.11 and L_{eff}=0.72 (see Sect. 4.2).

The resulting NO_2 TSCDs close to the source regions (mainly New Orleans and Houston) are apparently overestimated in the FLEXPART run. The main reason is probably that the assumed lifetime of 24 h is too long at ground (see above) what can easily explain a factor of 2.

Over the convective complex, on the other hand, the modelled anthropogenic NO_x TVCDs are low ($<2.5 \times 10^{15}$ molec/cm^2). The simulated anthropogenic NO_2 TSCDs, however, seem to generally underestimate the measured NO_2 TSCDs of the eastern GOME pixels, even north from 30° N. Possible reason might be that the emission inventory overestimates hot spots like New Orleans compared to the anthropogenic emissions smoothly distributed along the coast. We thus take the FLEXPART TSCD as lower limit for the actual TSCD due to anthropogenic emissions for pixels 1–9.

To derive an upper limit for the impact of anthropogenic NO_x we assume a maximum background level of anthropogenic NO_x TVCDs of 5×10^{15} molec/cm^2 over the considered area, i.e. twice as much as modelled by FLEXPART. This value corresponds to the NO_x TVSCD measured by GOME north from the convective complex for cloud free conditions, assuming an AMF of 1 and a NO_2/NO_x ratio of 0.5. Thereby, we ignore the probable decrease of anthropogenic NO_x levels southwards from the coast as detected for the western and middle GOME pixels. But even for an *actual* anthropogenic NO_x TVCD of 5×10^{15} molec/cm^2 at the eastern pixels, the expected *measured* NO_2 TSCD would be only 0.4×10^{15} molec/cm^2, since the strong shielding effect of the high and thick cloud cover leads to a conversion factor of 12.49 for anthropogenic NO_2 (see Sect. 4.2). The upper limit of anthropogenic NO_2 is thus below 5.8% of the actually detected TSCDs, while the lower limit, taking FLEXPART TSCDs, is half this value, i.e. 3.0%. We take the average, i.e. 4.4% as most probable value for the fraction of anthropogenic NO_x. The high NO_2 TSCDs in Fig. 1 can thus by no means be explained with transport of anthropogenic NO_x alone.

4.3.2 Aged LNO_x

Besides anthropogenic NO_x, aged LNO_x may contribute to the detected NO_2 plume as well. In fact, NLDN detected several flashes on 29 August west from Florida. However, as discussed in Sect. 3, part of this LNO_x is only transported to the southern part of the large complex on 30 August, while LNO_x in the northern part is freshly released.

The possible impact of aged LNO_x was estimated with FLEXPART using the NLDN flash counts from 27 August

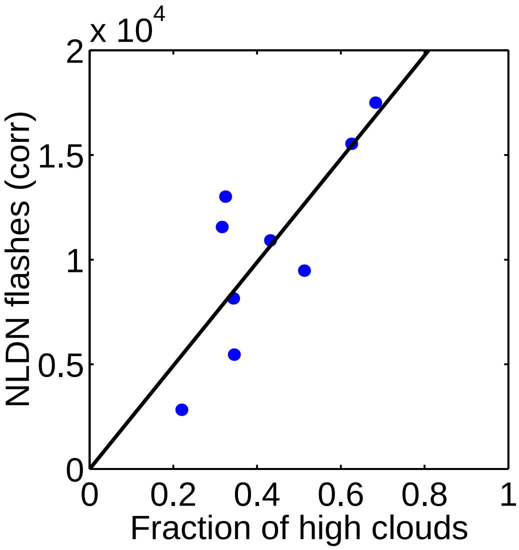

Fig. 7. Correlation of NLDN flash counts and the fraction of the GOME pixel covered with high clouds, i.e. having a CTT below 220 K, for pixels 1–9.

on. For every flash, a fixed amount of NO_2 (artificial units) was released in the respective grid box according to the vertical profile given by Table 2 (tropical marine) in Pickering et al. (1998). The e-folding lifetime was set to 4 days (Jaegle et al., 1998). This run was performed twice: the first run involves all flashes detected till 30 August, 16:48 UTC and stopped at 18:00 UTC (Fig. 6a). The second run simulates the same time period, but stops the release of fresh LNO_x on 30 August 0:00 UTC (Fig. 6b). I.e. run 1 shows the combination of aged and fresh LNO_x, while run 2 only considers aged LNO_x (i.e. LNO_x prior to 30 August). The comparison of both runs, i.e. the ratio of run 2 and run 1, allows to assess the fraction of aged LNO_x. For the LNO_x in the area covered by the GOME pixels 1–9, the fraction of LNO_x that is aged is 11%. It has to be noticed that this relative number depends neither on the assumptions about the LNO_x released per flash nor on the detection efficiency of NLDN.

4.3.3 Outflow of LNO_x

In the northern part of the convective complex, more than half of the flashes have occurred within 3 h before GOME measurement. But that also means that nearly half of the produced LNO_x is older than 3 h. Parts of the LNO_x produced in the area of GOME pixels 1–9 are thus transported outside. According to ECMWF windfields, main transport occurs in southerly direction. We estimate the amount of outflow using FLEXPART. Similar to the run performed in Sect. 4.3.2, the distribution of LNO_x was modelled by releasing an arbitrary fixed amount of LNO_x for every flash, starting from 30 August at 00:00 UTC with infinite lifetime. The resulting distribution of LNO_x is compared to the hypothetical distribution of LNO_x in the absence of transport, i.e. the distribution of the flash locations itself. The comparison reveals that 80% of the released LNO_x remained inside the GOME pixels 1–9.

The (small) contribution of anthropogenic NO_2 is subtracted from the measured NO_2 TSCDs prior to conversion to NO_x TVCDs (see Eq. 3). The effects of aged LNO_x and outflow of fresh LNO_x are accounted for by applying the correction factors c_{aged}=0.89 and c_{out}=1/0.8=1.25 that partly balance each other out. The overall uncertainty due to the different effects of transport is taken as 10%.

4.4 What is the total quantity of LNO_x produced?

The detected NO_2 plume can be directly assigned to the release of fresh LNO_x. Since the northern part of the convective complex is quite young (few hours), chemical decay of the produced LNO_x can be neglected due to the long lifetime of NO_x in the upper troposphere (Jaegle et al., 1998). Hence the detected NO_2 TSCDs can be converted directly to the LNO_x produced. Using Eq. (3), we derive a mean corrected NO_x TVCD of 3.0 (1.4–6.0)$\times10^{15}$ molec/cm^2.

To derive the total LNO_x produced in the convective complex north of 25° N, these TVCDs have to be integrated across the corresponding area A (see Eq. 2). The area of the convective system for pixels 1–9 is determined by counting the respective PMD subpixels with a HICRU CF>0.5. This results in 79 pixels of 20×40 km^2 each, i.e. 63200 km^2 in total. Integration of the NO_x TVCDs over the clouded area results in 3.1×10^7 moles of NO_x, corresponding to 4.4×10^5 kg [N], that are produced by this lightning event.

Combining both numbers, the total LNO_x release and the total number of flashes, results in a LNO_x production of 90 moles/flash, or 1.3 kg [N]/flash for this particular event. Errors are discussed in detail in Sect. 5.

4.5 The southern part

Combining measured NO_2 TSCDs and NLDN flash counts, we estimated the production of LNO_x for pixels 1–9. This approach is not feasible for pixels 10–14 due to low NLDN DE. Nevertheless, we give a rough estimate of LNO_x production for pixels 10–14 using the CTTs measured by GOES.

As lightning is caused by deep convection, flash rates have been found to be closely related to cloud top heights (Price and Rind, 1992). We use the fraction of the GOME pixels covered by clouds with a CTT below 220 K as proxy for high clouds. This temperature corresponds to a cloud top height above 12.5 km. Figure 7 displays the flashes detected by NLDN (scaled with respect to DE) relative to the fraction of high clouds for pixels 1–9. The correlation is R=0.79, and a linear fit (forced through zero) results in a slope of 2.47×10^4.

We use this relation for a simple estimate of the number of flashes for pixels 10–14, resulting in 5.4×10^4 flashes. The inflow of LNO_x from the northern part and the outflow of LNO_x from the southern part are difficult to quantify and partly cancel each other out. Effects of transport are thus neglected for our rough quantification of the southern part. Taking the same factors for IC/CG ratio and NO_x profile and partitioning as above, this results in a LNO_x production of 143 moles/flash. This number is about 50% higher than that derived for pixels 1–9. The main reason is probably an underestimation of the number of flashes for pixels 10–14, where lightning has taken place for several hours before the ERS-2 overpass (see Fig. 4), while the relation shown in Fig. 7 has been derived for the relatively young convective system covered by pixels 1–9.

5 Discussion

In our estimate, resulting in a LNO_x production of 90 moles/flash, several assumptions on different parameters are involved that are discussed in detail in the following.

The single errors/uncertainties are not gaussian and in particular not symmetric. We thus give a conservative error range for our estimation by considering the extreme values for the factors involved in Eqs. (2, 3), i.e. the number of flashes n (depending on the assumed IC/CG ratio), the estimated anthropogenic NO_2 SCD, the correction factors c_{cloud}, c_{aged} and c_{out}, and the conversion factor f. This results in a range of 32–240 moles/flash, i.e. 0.4–3.4 kg [N]/flash, for LNO_x production.

The climatological IC/CG ratio is a good first guess, but it has been reported in literature, that individual thunderstorms may show a very high IC/CG ratio of up to 100 (Dye et al., 2000). For such an extreme event, we would have underestimated the actual number of flashes drastically, thus overestimated the LNO_x production. However, such a scenario is rather unlikely, since the LIS measurement on 30 August, overpassing the detected convective system at 14:07–14:09 UTC, shows no increased number of flashes compared to NLDN.

The transport and uplift of anthropogenic NO_x has been simulated with FLEXPART using up to date emissions and an improved convection scheme. Nevertheless, we cannot rule out that the upward transport is underestimated by FLEXPART in particular for such a rapidly evolving system. If FLEXPART underestimates the amount of anthropogenic NO_x uplifted in the anvil, we would also underestimate the AMF for anthropogenic NO_x. But on the other hand, in this case the NO_x would be shifted towards NO and the assumed NO/NO_2 ratio for anthropogenic NO_x would have to be modified. For the extreme scenario of all anthropogenic NO_x lifted up and mixed homogeneously between 7 and 13 km, leading to an AMF of 0.90, and a NO_2/NO_x ratio of 0.26, anthropogenic NO_x still could only explain less than 20% of the observed NO_2 TCVDs.

Correction for the partly cloudy GOME pixels and consideration of aged LNO_x and outflow of fresh LNO_x only lead to small modifications with negligible errors.

The largest source of uncertainty is the conversion factor f, depending on NO_x profile/partitioning and box AMFs.

LNO_x profiles are taken from different cloud resolving model studies. The ensemble of different profiles allows to study the impact of the LNO_x profile on A_{eff}, L_{eff} and f. While the different profiles lead to variations in A_{eff} up to a factor of nearly 2, the effect on L_{eff} is rather small (30%). The uncertainty in f due to profile variations alone is below 25%.

The NO_x partitioning in thunderstorm clouds of geolocation, season, and local time similar to the lightning event under consideration was measured by Ridley et al. (1994, 1996). Since we cannot exclude that the actual NO_x partitioning differs for our case study, a large uncertainty range of 50% for L in the anvil region is assumed in Sect. 4.2.

Our calculations are based on box AMFs calculated for cumulonimbus clouds by Hild et al. (2002) that are given without errors. Strong deviations from these box AMFs would lead to significant variations in our calculated conversion factor. Hence further effort has to be put on additional box AMF calculations for cumulonimbus conditions with independent models.

Simple extrapolation of our estimated LNO_x production per flash, assuming a mean flash rate of 44 flashes per second globally (Christian et al., 2003), gives a global LNO_x production of 1.7 (0.6–4.7) Tg [N]/yr. This number is in good agreement with current literature values, but lower than the often cited number of 5 Tg [N]/yr. However, this particular event is not necessarily representative for global lightning.

Also other LNO_x estimates using GOME data result in rather low estimates (2.7 (0.8–14) Tg [N]/yr (Beirle et al., 2004c); 1.1–6.4 Tg [N]/yr (Boersma et al., 2004)). However, the remaining uncertainties are yet too high to state the annual LNO_x production being significantly lower than 5 Tg [N]. Further case studies and statistical evaluations of LNO_x from satellite measurements are necessary to reduce current uncertainties.

6 Conclusions and outlook

In the past, GOME NO_2 data has been used to estimate LNO_x production by statistical approaches (Beirle et al., 2004a; Boersma et al., 2005). The direct observation of active convective systems, however, has several advantages: Due to deep convection, the NO_x is lifted up to the cloud top, where satellite measurements are quite sensitive for it. The LNO_x plume is not yet diluted, hence local NO_x levels are high. Spatial patterns can be identified and compared to flash rate patterns. And shortly after the LNO_x production, its chemical loss is rather negligible, simplifying the calculation of the total NO_x production.

Within this study, we could identify NO_x from lightning with GOME data for a particular convective system, matching the GOME observation in space and time. The LNO_x produced is estimated as 90 (32–240) moles of NO_x per flash, corresponding to 1.7 (0.6–4.7) Tg [N]/yr globally. This case study impressively illustrates the fundamental feasibility of LNO_x detection and quantification with satellite NO_2 measurements. Hence space borne spectrometers provide a new and independent approach for the estimation of LNO_x.

The lightning data from NLDN is limited to the USA, where anthropogenic sources are often interfering with the quantification of LNO_x. The recently established World Wide Lightning Location Network WWLLN (Lay et al., 2004), as well as the long-range lightning detection networks operated by Vaisala (Pessi et al., 2004; Demetriades et al., 2005), will allow similar case studies to be carried out on a global scale and hence to fully use the potential of satellite data. Since WWLLN is partly sensitive to IC flashes, the uncertainty arising from the IC/CG ratio used is also reduced.

In the future, similar case studies will be performed systematically using the improved spatial resolution of the SCanning Imaging Absorption SpectroMeter for Atmospheric CHartographY SCIAMACHY, the Ozone Monitoring Instrument OMI, and the GOME successor GOME-2. Of particular interest will be the analysis of LNO_x plumes from strong convective systems that are subsequently overpassed by different satellite instruments, e.g. GOME-2 (9:30 a.m.), SCIAMACHY (10:00 a.m.) and OMI (1.45 p.m.). Such scenarios allow the study of LNO_x plume evolution that holds – if combined with meteorological data – valuable information on LNO_x profile, NO_x lifetime, and the LNO_x produced in thunderstorms.

For the reduction of errors, it would be a milestone to have simultaneous measurements from aircraft (providing NO_x profile and NO_x partitioning) and satellite (capturing the whole system at once) for a strong convective complex.

Further efforts will have to be assigned to the modeling of radiative transfer and the calculation of AMFs for fresh LNO_x in thunderstorm clouds.

Appendix A

Correction for partly clouded pixels

The GOME NO_2 measurements are taken with a rather large footprint of $320\times40\,\mathrm{km}^2$, hence they represent mean SCDs of generally inhomogeneous NO_2 distributions and cloud fractions.

To estimate the SCD above the convective complex, we assume the GOME pixels to be divided in a cloud free and a totally clouded part. Let f be the fraction of the pixel being clouded, S_0 the true SCD for the cloud free part and S_c the true SCD for the clouded part of the GOME pixel. The total SCD S measured by GOME is the mean of S_0 and S_c weighted by the area and the brightness of the cloud free and the clouded part, respectively:

$$S = \frac{I_c \cdot f \cdot S_c + I_0 \cdot (1-f) \cdot S_0}{I_c \cdot f + I_0 \cdot (1-f)}\,, \tag{A1}$$

where I_c and I_0 are the intensities one would measure for a totally clouded/cloud free scene, respectively. Solving Eq. (A1) for S_c, the true SCD over the clouded part is

$$S_c = S + \frac{I_0}{I_c} \cdot \frac{1-f}{f} \cdot (S - S_0)\;. \tag{A2}$$

The ratio I_0/I_c is gained by comparing the maximum and minimum intensities of the PMD subpixels in the blue spectral range, resulting in I_c=7×I_0. S_0 is estimated taking the SCD of the respective neighboring, cloud free center GOME pixel. With these numbers, S_c is on average higher than S by 5% for pixels 1–9. The measured SCD S has thus to be corrected by a factor of 1.05. The extreme cases of $S_{0,\mathrm{min}}=0$ and $S_{0,\mathrm{max}}=3\times10^{15}$ (i.e. the maximum SCD of the center GOME pixels) lead to a range of 1.04–1.10 for the correction factor c_{cloud}.

Appendix B

Effective AMF and NO_2/NO_x partitioning

The troposphere is divided into n layers. Let a_i be the box AMF, $s_i^{NO_2}$ and $v_i^{NO_2}$ the slant/vertical column of NO_2 and $v_i^{NO_x}$ the vertical column of NO_x of the ith layer. Furthermore, l_i is the ratio $v_i^{NO_2}/v_i^{NO_x}$, and $p_i^{NO_x}$ and $p_i^{NO_2}$ represent the normalized profiles of NO_x and NO_2, respectively.

The total TSCD of NO_2, S^{NO_2}, can be expressed as

$$S^{NO_2}=\sum s_i^{NO_2}=\sum v_i^{NO_2}\cdot a_i=V^{NO_2}\cdot\sum p_i^{NO_2}\cdot a_i \tag{B1}$$

The latter is the sum of the box AMFs weighted with the vertical NO_2 profile, resulting in the effective AMF:

$$A_{\mathrm{eff}} = \sum p_i^{NO_2}\cdot a_i \tag{B2}$$

On the other hand, S can be expressed as

$$\begin{aligned} S^{NO_2} &= \sum v_i^{NO_2}\cdot a_i = \sum l_i \cdot v_i^{NO_x}\cdot a_i \\ &= V^{NO_x}\cdot \sum p_i^{NO_x}\cdot l_i \cdot a_i \end{aligned} \tag{B3}$$

$$\Rightarrow V^{NO_x} = \frac{S^{NO_2}}{\sum p_i^{NO_x}\cdot l_i\cdot a_i} = f\cdot S^{NO_2} \tag{B4}$$

with

$$f = \frac{1}{\sum p_i^{NO_x}\cdot l_i\cdot a_i}\,. \tag{B5}$$

Alternatively, f can be written as

$$f \overset{(B4)}{=} \frac{V^{NO_x}}{S^{NO_2}} \overset{(B1)}{=} \frac{V^{NO_x}}{V^{NO_2}\cdot A_{eff}} = \frac{1}{\frac{V^{NO_2}}{V^{NO_x}}\cdot A_{eff}} = \frac{1}{L_{eff}\cdot A_{eff}} \quad (B6)$$

with

$$L_{eff} := \frac{V^{NO_2}}{V^{NO_x}}\,. \quad (B7)$$

Hence, L_{eff} can be calculated as

$$L_{eff} \overset{(B6)}{=} \frac{1}{f\cdot A_{eff}} \overset{(B5)}{=} \frac{\sum p_i^{NO_x}\cdot l_i\cdot a_i}{A_{eff}} \overset{(B2)}{=} \frac{\sum p_i^{NO_x}\cdot a_i\cdot l_i}{\sum p_i^{NO_2}\cdot a_i}\,. \quad (B8)$$

This can be interpreted as weighted sum of the NO_x partitionings of the single layers.

A_{eff} and L_{eff} are calculated in Sect. 4.2. for illustration. For the final conversion (Eq. 3) and the estimation of errors, Eq. (B5) is used for the calculation of f, since modifications of $p_i^{NO_x}$, l_i and a_i affect both A_{eff} and L_{eff}, but effects partly cancel out in f.

Acknowledgements. This study was funded by the German Ministry for Education and Research as part of the NOXTRAM project (Atmospheric Research 2000). We would like to thank the European Space Agency (ESA) operation center in Frascati (Italy) and the "Deutsches Zentrum für Luft- und Raumfahrt" DLR (Germany) for providing GOME spectra. We thank the "Deutscher Wetterdienst" for kindly providing access to ECMWF. GOES-8 satellite images were kindly provided by UNIDATA internet delivery. We thank S. A. McKeen and G. J. Frost from NOAA for making available their inventory of anthropogenic emissions in North America in a format suitable for incorporation into FLEXPART. We acknowledge the constructive comments of two anonymous reviewers.

Edited by: A. Richter

References

Beirle, S., Platt, U., Wenig, M., and Wagner, T.: Weekly cycle of NO_2 by GOME measurements: a signature of anthropogenic sources, Atmos. Chem. Phys., 3, 2225–2232, 2003.

Beirle, S., Platt, U., Wenig, M., and Wagner, T.: NO_x production by lightning estimated with GOME, Adv. Space Res., 34(4), 793–797, 2004a.

Beirle, S., Platt, U., Wenig, M., and Wagner, T.: Highly resolved global distribution of tropospheric NO_2 using GOME narrow swath mode data, Atmos. Chem. Phys., 4, 1913–1924, 2004b.

Beirle, S., Platt, U., von Glasow, R., Wenig, M., and Wagner, T.: Estimate of nitrogen oxide emissions from shipping by satellite remote sensing, Geophys. Res. Lett., 31, L18102, doi:10.1029/2004GL020312, 2004c.

Boccippio, D. J., Cummins, K. L., Christian, H. J., and Goodman, S. J.: Combined Satellite- and Surface-Based Estimation of the Intracloud-Cloud-to-Ground Lightning Ratio over the Continental United States, Mon. Wea. Rev., 129, 108–122, 2000.

Boersma, K. F., Eskes, H. J., and Brinksma, E. J.: Error analysis for tropospheric NO_2 retrieval from space, J. Geophys. Res., 109, D04311, doi:10.1029/2003JD003962, 2004.

Boersma, K. F., Eskes, H. J., Meijer, E. W., and Kelder, H. M.: Estimates of lightning NO_x production from GOME satellite observations, Atmos. Chem. Phys., 5, 2311–2331, 2005.

Burrows, J., Weber, M., Buchwitz, M., Rozanov, V. V., Ladstädter-Weissenmayer, A., Richter, A., de Beek, R., Hoogen, R., Bramstedt, K., Eichmann, K.-U., Eisinger, M., and Perner, D.: The Global Ozone Monitoring Experiment (GOME): Mission concept and first scientific results, J. Atmos. Sci., 56, 151–175, 1999.

Choi, Y., Wang, Y., Zeng, T., Martin, R. V., Kurosu, T. P., and Chance, K.: Evidence of light- lightning NO_x and convective transport of pollutants in satellite observations over North America, Geophys. Res. Lett., 32, L02805, doi:10.1029/2004GL021436, 2005.

Christian, H. J., Blakeslee, R. J., Boccippio, D. J., Boeck, W. L., Buechler, D. E., Driscoll, K. T., Goodman, S. J., Hall, J. M., Koshak, W. J., Mach, D. M., and Stewart, M. F.: Global frequency and distribution of lightning as observed from space by the Optical Transient Detector, J. Geophys. Res., 108(D1), 4005, doi:10.1029/2002JD002347, 2003.

Cummins, K. L., Murphy, M. J., Bardo, E. A., Hiscox, W. L., Pyle, R. B., and Pifer, A. E.: A combined TOA/MDF technology upgrade of the U.S. National Lightning Detection Network, J. Geophys. Res., 103(D8), 9035–9044, doi:10.1029/98JD00153, 1998.

Demetriades, N. W. S., Murphy, M. J., and Holle, R. L.: Long range lightning nowcasting applications for meteorology, in: World weather research program symposium, Toulouse, France, 2005.

Dye, J. E., Ridley, B. A., Skamarock, W., Barth, M., Venticinque, M., Defer, E., Blanchet, P., Thery, C., Laroche, P., Baumann, K., Hubler, G., Parrish, D. D., Ryerson, T., Trainer, M., Frost, G., Holloway, J. S., Matejka, T., Bartels, D., Fehsenfeld, F. C., Tuck, A., Rutledge, S. A., Lang, T., Stith, J., and Zerr, R.: An overview of the Stratospheric-Tropospheric Experiment: Radiation, Aerosols and Ozone (STERAO)-Deep Convection experiment with result from the July 10, 1996 storm, J. Geophys. Res., 105, 10 023–10 045, 2000.

ECMWF: User Guide to ECMWF Products 2.1, Meteorological Bulletin M3.2, Reading, UK, 1995.

Emanuel, K. A.: A scheme for representing cumulus convection in large-scale models, J. Atmos. Sci., 48, 2313–2335, 1991.

Emanuel, K. A. and Zivkovic-Rothman, M.: Development and evaluation of a convection scheme for use in climate models, J. Atmos. Sci., 56, 1766–1782, 1999.

Fehr, T., Höller, H., and Huntrieser, H.: Model study on production and transport of lightning-produced NO_x in a EULINOX supercell storm, J. Geophys. Res., 109, D09102, doi:10.1029/2003JD003935, 2004.

Frost, G. and McKeen, S. A.: Emission inventory mapviewer, http://map.ngdc.noaa.gov/website/al/emissions/viewer.htm, 2004.

Frost, G. J., McKeen, S. A., Trainer, M., Ryerson, T. B., Holloway, J. S., Sueper, D. T., Fortin, T., Parrish, D. D., Fehsenfeld, F. C., Peckham, S. E., Grell, G. A., Kowal, D., Cartwright, J., Auerbach, N., and Habermann, T.: Effects of Changing Power Plant NO_x Emissions on Ozone in the Eastern United States, J. Geophys. Res., in press, 2006.

Grzegorski, M., Wenig, M., Platt, U., Stammes, P., Fournier, N., and Wagner, T.: The Heidelberg iterative cloud retrieval utilities

(HICRU) and its application to GOME data, Atmos. Chem. Phys. Discuss., 6, 1637–1678, 2006.

Hild, L., Richter, A., and Burrows, J. P.: Measurements of lightning-produced NO_2 by GOME and LIS, Symposium 2000 in Göteburg – Session: Atmosphere UV Radiation, Trace Gases Other Than Ozone, ID Nr. 349, 2000.

Hild, L., Richter, A., Rozanov, V., and Burrows, J. P.: Air Mass Calculations for GOME Measurements of lightning-produced NO_2, Adv. Space Res., 29(11), 1685–1690, 2002.

Huntrieser, H., Schlager, H., Feigl, C., and Höller, H.: Transport and production of NO_x in electrified thunderstorms: Survey of previous studies and new observations at midlatitudes, J. Geophys. Res., 103, 28 247–28 264, 1998.

Huntrieser, H., Feigl, C., Schlager, H., Schröder. F., Gerbig, C., van Velthoven, P., Flatoy, F., Thery, C., Petzold, A., Höller, H., and Schumann, U.: Airborne measurements of NO_x, tracer species, and small particles during the European Lightning Nitrogen Oxides Experiment, J. Geophys. Res., 107, doi:10.1029/2000JD000209, 2002.

Jaeglé, L., Jacob, D. J., Wang, Y., Weinheimer, A. J., Ridley, B. A., Campos, T. L., Sachse, G. W., and Hagen, D.: Sources and chemistry of NO_x in the upper troposphere over the United States, Geophys. Res. Lett., 25, 1709–1712, 1998.

Jaeglé, L., Martin, R. V., Chance, K., Steinberger, L., Kurosu, T. P., Jacob, D. J., Modi, A. I., Yoboue, V., Sigha-Nkamdjou, L., and Galy-Lacaux, C.: Satellite mapping of rain-induced nitric oxide emissions from soils, J. Geophys. Res., 109, D21310, doi:10.1029/2004JD004787, 2004.

Jourdain, L. and Hauglustaine, D.: The global distribution of lightning NO_x simulated on-line in a General Circulation Model, Phys. Chem. Earth (C), 26, 585–591, 2001.

Labrador, L. J., von Kuhlmann, R., and Lawrence, M. G.: Strong sensitivity of the global mean OH concentration and the tropospheric oxidizing efficiency to the source of NO_x from lightning, Geophys. Res. Lett., 31, L06102, doi:10.1029/2003GL019229, 2004.

Lay, E. H., Holzworth, R. H., Rodger, C. J., Thomas, J. N., Pinto Jr, O., and Dowden, R. L.: WWLL global lightning detection system: Regional validation study in Brazil, Geophys. Res. Lett., 31(3), L03102, doi:10.1029/2003GL01888203, 2004.

Lee, D. S., Köhler, I., Grobler, E., Rohrer, F., Sausen, R., Gallardo-Klenner, L., Olivier, J. G. J., Dentener, F. J., and Bouwman, A. F.: Estimations of global NO_x emissions and their uncertainties, Atmos. Environ., 31, 1735–1749, 1997.

Leue, C., Wenig, M., Wagner, T., Klimm, O., Platt, U., and Jähne, B.: Quantitative analysis of NO_2 emissions from GOME satellite image sequences, J. Geophys. Res., 106, 5493–5505, 2001.

Levy II, H., Moxim, W. J., and Kasibhatla, P. S.: A global three-dimensional time-dependent lightning source of tropospheric NO_x, J. Geophys. Res., 101(D17), 22 911–22 922, doi:10.1029/96JD02341, 1996.

Martin, R. V., Chance, K., Jacob, D. J., Kurosu, T. P., Spurr, R. J. D., Bucsela, E., Gleason, J. F., Palmer, P. I., Bey, I., Fiore, A. M., Li, Q., Yantosca, R. M., and Koelemeijer, R. B. A.: An improved retrieval of tropospheric nitrogen dioxide from GOME, J. Geophys. Res., 107(D20), 4437, doi:10.1029/2001JD001027, 2002.

Martin, R. V., Jacob, D. J., Chance, K., Kurosu, T. P., Palmer, P. I., and Evans, M. J.: Global inventory of nitrogen oxide emissions constrained by space-based observations of NO_2 columns, J. Geophys. Res., 108, 4537, doi:10.1029/2003JD003453, 2003.

Nesbitt, S. W., Zhang, R., and Orville, R. E.: Seasonal and global NO_x production by lightning estimated from the Optical Transient Detector (OTD), Tellus, 52B, 1206–1215, 2000.

Pessi, A., Businger, S., Cummins, K. L., and Turner, T.: On the relationship between lightning and convective rainfall over the central pacific ocean, in: ILDC 2004 18th International Lightning Detection Conference, http://www.soest.hawaii.edu/MET/Faculty/businger/personnel/pessi/Pessi-Pacnet.doc, ref. no. 21, Helsinki, Finland, 2004.

Pickering, K. E., Wang, Y., Tao, W.-K., Price, C., and Müller, J.-F.: Vertical distributions of lightning NO_x for use in regional and global chemical transport models, J. Geophys. Res., 103, 31 203–31 216, 1998.

Platt, U.: Differential optical absorption spectroscopy (DOAS), in: Air Monitoring by Spectrometric Techniques, edited by: Sigrist, M., John Wilsy, New York, pp. 27–84, 1994.

Price, C. and Rind, D.: A Simple lightning parameterization for calculating global lightning distributions, J. Geophys. Res., 97(D9), 9919–9933, doi:10.1029/92JD00719, 1992.

Price, C., Penner, J., and Prather, M., NO_x from lightning (1). Global distribution based on lightning physics, J. Geophys. Res., 102, 5929–5941, 1997.

Ridley, B. A., Dye, J. E., Walega, J. G., Zheng, J., Grahek, F. E., and Rison, W.: On the production of active nitrogen by thunderstorms over New Mexico, J. Geophys. Res., 101, 20 985–21 005, 1996.

Richter, A. and Burrows, J.: Retrieval of Tropospheric NO_2 from GOME Measurements, Adv. Space Res., 29(11), 1673–1683, 2002.

Richter, A., Eyring, V., Burrows, J. P., Bovensmann, H., Lauer, A., Sierk, B., and Crutzen, P. J.: Satellite measurements of NO_2 from international shipping emissions, Geophys. Res. Lett., 31, L23110, doi:10.1029/2004GL020822, 2004.

Solomon, S., Schmeltekopf, A. L., and Sanders, R. W.: On the interpretation of zenith sky absorption measurements, J. Geophys. Res., 92, 8311–8319, 1987.

Spichtinger, N., Wenig, M., James, P., Platt, U., and Stohl, A.: Satellite detection of a continental-scale plume of nitrogen oxides from boreal forest fires, Geophys. Res. Lett., 28, 4579–4582, 2001.

Spichtinger, N., Damoah, R., Eckhardt, S., Forster, C., James, P., Beirle, S., Wagner, T., Novelli, P. C., and Stohl, A.: Boreal forest fires in 1997 and 1998: a seasonal comparison using transport model simulations and measurement data, Atmos. Chem. Phys., 4, 1857–1868, 2004.

Stockwell, D. Z., Giannakopoulos, C., Plantevin, P.-H., Carver, G. D., Chipperfield, M. P., Law, K. S., Pyle, J. A., Shallcross, D. E., and Wang, K.-Y.: Modelling NO_x from lightning and its impact on global chemical fields, Atmos. Environ., 33, 4477–4493, 1999.

Stohl, A., Hittenberger, M., and Wotawa, G.: Validation of the Lagrangian particle dispersion model FLEXPART against large scale tracer experiment data, Atmos. Environ., 32, 4245–4264, 1998.

Stohl, A., Huntrieser, H., Richter, A., Beirle, S., Cooper, O. R., Eckhardt, S., Forster, C., James, P., Spichtinger, N., Wenig, M., Wagner, T., Burrows, J. P., and Platt, U.: Rapid intercontinental air pollution transport associated with a meteorological bomb, Atmos. Chem. Phys., 3, 969–985, 2003.

Stohl, A., Forster, C., Frank, A., Seibert, P., and Wotawa, G.: Technical note: The Lagrangian particle dispersion model FLEXPART version 6.2, Atmos. Chem. Phys., 5, 2461–2474, 2005.

Tie, X., Zhang, R., Brasseur, G., and Lei, W.: Global NO_x production by lightning, J. Atmos. Chem., 43, 61–74, 2002.

U.S. EPA: EPA Clearinghouse for inventories and emissions factors: 1999 National Emission Inventory Documentation and Data – Final Version 3.0, http://www.epa.gov/ttn/chief/net/1999inventory.html, 2004a.

U.S. EPA: EPA Clearinghouse for inventories and emissions factors: Related Spatial Allocation Files – "New" Surrogates; http://www.epa.gov/ttn/chief/emch/spatial/newsurrogate.html, 2004b.

Velders, G. J. M., Granier, C., Portmann, R. W., Pfeilsticker, K., Wenig, M., Wagner, T., Platt, U., Richter, A., and Burrows, J.: Global tropospheric NO_2 column distributions: Comparing 3-D model calculations with GOME measurements, J. Geophys. Res., 106, 12 643–12 660, 2001.

Wagner, T.: Satellite observations of atmospheric halogen oxides, PhD thesis, University of Heidelberg, http://www.ub.uni-heidelberg.de/archiv/539, 1999.

Wenig, M., Spichtinger, N., Stohl, A., Held, G., Beirle, S., Wagner, T., Jähne, B., and Platt, U.: Intercontinental transport of nitrogen oxide pollution plumes, Atmos. Chem. Phys., 3, 387–393, 2003.

Zhang, R., Sanger, N. T., Orville, R. E., Tie, X., Randel, W., and Williams, E. R.: Enhanced NO_x by lightning in the upper troposphere and lower stratosphere inferred from the UARS global NO_2 measurements, Geophys. Res. Lett., 27, 685–688, 2000.